Molecular Architecture of *Escherichia coli* F_1 Adenosinetriphosphatase†

Edward P. Gogol, Uwe Lücken,‡ Tracie Bork, and Roderick A. Capaldi*

Institute of Molecular Biology, University of Oregon, Eugene, Oregon 97403

Received November 9, 1988; Revised Manuscript Received January 30, 1989

ABSTRACT: The structure of the *E. coli* F_1 ATPase (ECF_1) has been studied by a novel combination of two specimen preparation and image analysis techniques. The molecular outline of the ECF_1 was determined by three-dimensional reconstruction of images of negatively stained two-dimensional crystals of ECF_1. Internal features were revealed by analysis of single particles of ECF_1, preserved in their native state in a thin layer of amorphous ice, and examined by cryoelectron microscopy. Various projections of the unstained ECF_1 were interpreted consistently with the three-dimensional structure in negative stain, yielding a more informative description of the enzyme than otherwise possible. Results show that the ECF_1 is a roughly spherical complex ~90–100 Å in diameter. Six elongated protein densities (the α and β subunits, each ~90 Å × ~30 Å in size) comprise its hexagonally modulated periphery. At the center of the ECF_1 is an aqueous cavity which extends nearly or entirely through the length of the complex. A compact protein density, located at one end of the hexagonal barrel and closely associated with one of the peripheral subunits, partially obstructs the central cavity.

The membrane-bound proton-translocating ATPase or F_1F_0 is a large multisubunit complex responsible for ATP synthesis in oxidative phosphorylation and photophosphorylation and for ATP-driven generation of a transmembrane proton gradient (Vignais & Satre, 1984; Senior, 1988). The enzyme is ubiquitous, being present in mitochondria of both plants and animals, in chloroplasts of plants, and in the plasma membrane of bacteria. The simplest F_1F_0-type ATPases in structural terms are those of bacterial origin. The *Escherichia coli* enzyme (ECF_1F_0) is composed of 8 different subunits (Foster & Fillingame, 1979; Walker et al., 1984), compared with 13 or more in F_1F_0 from mammalian sources (Ludwig et al., 1980; Amzel & Pedersen, 1983). The F_1 sector (ECF_1) is the catalytic part of the complex. It is composed of five different subunits (α, β, γ, δ, and ϵ) in the molar ratio of 3:3:1:1:1 and with a molecular weight of 381 000 (Foster & Fillingame, 1982; Walker et al., 1984). There are three catalytic sites per molecule which have been localized to β subunits (Vignais & Lunardi, 1985). The F_0 part is the transmembrane portion of the complex, composed of three different subunits (a, b, and c) in the molar ratio 1:2:(10–12) (Foster & Fillingame, 1979). The F_0 part forms a proton pore when reconstituted into membranes (Schneider & Altendorf, 1985).

The structure of the F_1 isolated from a variety of sources has been studied by using both biochemical and biophysical techniques [reviewed in Amzel and Pedersen (1983)]. Electron microscopy has been particularly useful in defining the gross features of the protein complex [reviewed in Brink et al. (1988)]. Molecules of F_1 in negatively stained preparations are usually found in one predominant orientation, which shows a hexagonal arrangement of six equal-sized lobes, presumably representing the three α and three β subunits (Akey et al., 1983; Tiedge et al., 1983; Tsuprun et al., 1984; Boekema et al., 1988). A seventh density, either centrally or asymmetrically located, has also been observed (Boekema et al., 1986).

Analysis of single dispersed particles, as discussed above, provides a projection view of the protein from one (or several) directions, but interpretation of the three-dimensional structure with this approach is not straightforward. In specimens arranged as two-dimensional crystals, images can be recorded at different tilt angles and then combined by Fourier methods to yield a three-dimensional map of the protein (Amos et al., 1982). Two-dimensional crystals have been obtained with F_1 from thermophilic bacteria (Kagawa et al., 1976) but these were not suitable for a three-dimensional structural determination.

We are studying the structure of ECF_1F_0 by electron microscopy, both by direct methods and by labeling with subunit-specific monoclonal antibodies. As a first step, we have obtained two-dimensional crystals of the F_1 portion of the complex and have determined a three-dimensional structure in negative stain. This analysis provides the molecular outline of the complex. Our work has been extended by single-particle analysis of unstained ECF_1 using cryoelectron microscopy. Projection images of ECF_1 rapidly frozen in a layer of ice have been collected, sorted, and averaged; while many of the individual images are not readily interpretable, major classes of views are consistent with the three-dimensional structure derived from the analysis of the negatively stained crystals. These images provide information about the center of the molecule, which was not defined in the negatively stained preparations.

Materials and Methods

Preparation and Reconstitution of the Enzyme. ECF_1F_0 was prepared and reconstituted into membrane structures as previously described (Aggeler et al., 1987). Reconstituted preparations had ATPase activities of 12–14 units/mg of protein when measured according to Lotscher et al. (1984) which were stimulated 3.5–4.5-fold by 0.5% *N*,*N*-dimethyldodecylamine *N*-oxide (LDAO; Fluka). The activity was 90–95% inhibited by reaction with 20 μM DCCD at room temperature for 1 h, and this inhibition was fully reversible by addition of LDAO. Preparations were kept at 0–4 °C for up to 10 days before use.

†This work was funded by NIH Grants HL 24526 and GM 39806 to R.A.C. and NATO Training Fellowship 300-402-5036 from the DAAD to U.L. Microscopy facilities were funded by NIH Grant RR 02756-01.

‡Present address: Fritz-Haber-Institut der Max-Planck-Gesellschaft, Faradagweg 4-6, D-1000 Berlin 33, Federal Republic of Germany.

0006-2960/89/0428-4709$01.50/0

ECF_1 was prepared by the procedure of Wise et al. (1984), with ion-exchange chromatography performed on a DEAE-Sephadex CL-6B column (Sigma), using a linear NaCl gradient (40–325 mM) and maintaining a high protein concentration to prevent dissociation of the ϵ subunit. The final purification step involved gel filtration on Sephacryl S-300 (Pharmacia) in the presence of 50 mM Tris-HCl (pH 7.5), 1 mM dithioerythritol, 2 mM ATP, 0.5 mM ethylenediaminetetraacetic acid, and 20% glycerol. The protein concentration on the column was kept above 2 mg/mL. This method generates an enzyme with all five subunits clearly visualized by Coomassie blue staining. Protein concentrations were measured by the method of Bradford (1976).

Microscopy and Analysis of Negatively Stained Specimens. Two-dimensional arrays of ECF_1 were formed by applying reconstituted ECF_1F_0 preparations (in dialysis buffer) to carbon-coated electron microscope grids, washing briefly with three drops of 2% phosphotungstic acid (PTA) (pH 7.0), and drying in air at room temperature. Identical arrays were also formed, though with lower frequency, when ECF_1 was similarly applied and negatively stained.

Specimens were examined and images were recorded with a Philips CM12 electron microscope equipped with a tilting goniometer. Grids were mounted in the specimen holder in a consistent orientation (specimen facing downward in the column), and images were recorded at 100 kV at a magnification of 35000×, using minimal dose methods (estimated electron dose of $\sim 8\ e^-/Å^2$). Images were usually recorded in pairs, including a zero or low tilt (<15°) along with each tilted (15–60°) image, on Kodak SO163 film and developed in full-strength Kodak developer D19 for 12 min. Higher tilts were obtained by using bent grids. Second or third images recorded under these conditions from a single area, from either tilted or untilted specimens, showed no sign of radiation damage.

Images were examined by optical diffraction for degree of underfocus, lack of astigmatism, and intensity and resolution of the crystalline diffraction pattern. Selected areas were digitized by microdensitometry (Optronics P1000), using a 25-μm step and spot size, corresponding to a sampling of 7.1 Å at the specimen. The numerical image arrays were Fourier transformed, amplitude peaks were located, and their positions were iteratively fitted to a lattice. Lattice distortions in each image (including tilted specimens) were minimized by applying the interpolative procedure of Henderson et al. (1986).

The Fourier terms from 44 images, spanning a tilt range of 0–66°, were cumulatively combined in the *p3* two-sided plane group. The in-plane resolution of the data (untilted specimens) was 24 Å [the (1,3) spots] and extended to approximately 30 Å in the perpendicular direction. Phase values within a range of 0.00125 $Å^{-1}$ along lattice rods were compared, yielding an average phase error of 21° for the 727 (out of 867 total) independent values entering the comparison. Curves were fitted to the data along the lattice lines by a weighted least-squares method (Agard et al., 1983), and Fourier terms for synthesis of a three-dimensional map were obtained by sampling the curves at intervals of 0.00125 $Å^{-1}$.

Cryoelectron Microscopy and Single-Particle Analysis. Frozen hydrated specimens were prepared by rapidly plunging thin films of buffered ECF_1 solutions at 4 °C into liquid ethane cooled to just above its freezing point. Aliquots (3–5 μL) of F_1 (~0.02–1.0 mg/mL) in isolation/storage buffer were applied to 400-mesh copper grids covered with holey carbon films, which had been made hydrophilic by glow discharge in air. Most of the sample was blotted away with filter paper, leaving films of solution over many of the holes, and the grids were dropped into nearly solidified ethane cooled with liquid nitrogen. The grids were transferred to and stored under liquid nitrogen until use.

Grids containing frozen samples were loaded under liquid nitrogen into a Gatan cold stage. Images were recorded with a Philips CM12 electron microscope as with the crystalline samples, but at a magnification of 57000×, with an electron dose of $\sim 20\ e/Å^2$, and at a defocus of 0.9 μm.

Micrographs were selected for image analysis by the absence of optical artifacts and the presence of adequate numbers of nonoverlapped ECF_1 particles in areas of thin ice over holes in the carbon support film. Selected areas of the films were digitized as described for the negatively stained specimens, using a 25-μm raster, corresponding to a sampling of 4.4 Å. Images were displayed on a raster graphics terminal, and 32 by 32 pixel areas (141 by 141 Å) approximately centered on particles were windowed by using the SPIDER image processing programs (Frank et al., 1981a). Each image was circularly masked to reduce surrounding background, Fourier low-pass-filtered at a resolution of 20 Å to further reduce image noise, and repeatedly aligned to selected reference images, described below, using auto- and cross-correlation procedures (Frank et al., 1981b).

A total of 1400 images of ECF_1 molecules were initially selected for processing, from 8 micrographs of 4 different preparations of the enzyme. Several clear images of distinctive views were used as initial references for alignment. Subsets of particles which both visually resembled and correlated well to the best initial references (ones to which many particles aligned) were averaged to use as new reference images in further rounds of alignment. Particles were manually classified as representatives of these views by the combined criteria of stable alignment, visual appearance, and relatively high correlation coefficient. Correspondence analysis based particle classification (Bretaudiere & Frank, 1986) was also attempted, using both the SPIDER (Frank et al., 1981a) and IMAGIC (van Heel & Keegstra, 1981) image analysis program packages.

RESULTS

Preparation of Two-Dimensional Crystals of ECF_1. Ordered arrays of ECF_1 have been observed with different preparations of enzyme and with different staining techniques. Two-dimensional crystals were occasionally obtained from isolated ECF_1 by applying the protein to carbon-coated electron microscopy grids in a solution of 2% PTA at neutral pH (Figure 1A). The frequency with which these arrays were seen could be increased by briefly washing the samples (on the grid) with 10% glycerol immediately before being exposed to the negative stain.

Ordered arrays were obtained more routinely when the intact ECF_1F_0, reconstituted into membranes, was applied to grids under the same staining conditions. A typical electron micrograph of one of these preparations is shown in Figure 1B. Crystalline arrays are present, along with free ECF_1 and membrane vesicles partially stripped of ECF_1 particles, dissociated from the F_0 by exposure to the heavy-metal salt. The stripping of F_1 from F_0 by high concentrations of PTA (1% or more) has been previously described by Racker et al. (1969).

Two-dimensional arrays of ECF_1 were also obtained by negatively staining membrane-bound ECF_1F_0 with PTA on a mica surface, coating them with a layer of carbon, and then restaining by floating the sample off in a solution of uranyl acetate (U. Lücken and R. A. Capaldi, unpublished results). These crystals were less frequent and not as well-ordered as those obtained by conventional staining with PTA alone. None

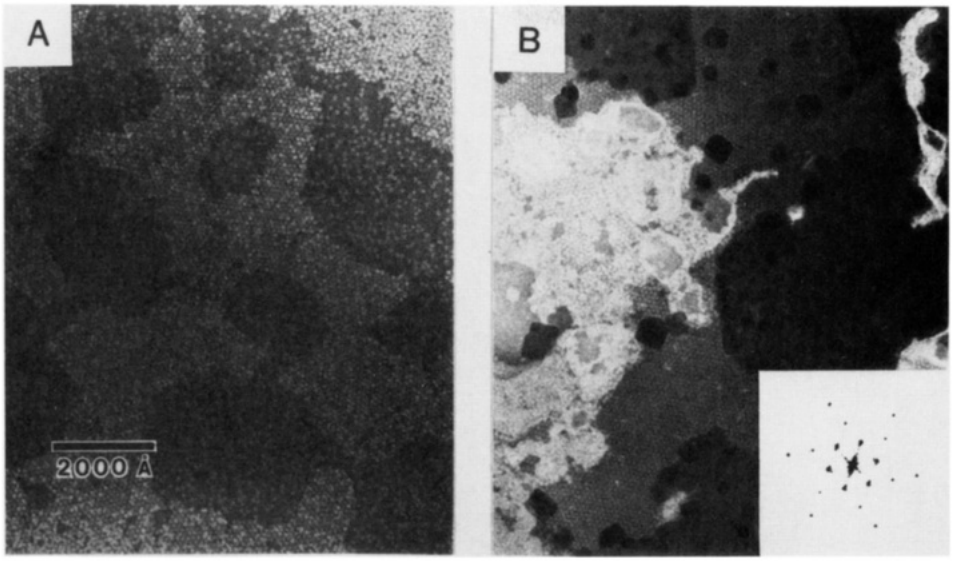

FIGURE 1: Electron micrographs of two dimensional crystalline arrays of ECF_1, stained with PTA, formed from isolated ECF_1 (A) and ECF_1F_0 (B). Note the free ECF_1 particles in (A) and the membranous ECF_1F_0 at the left center of (B). Inset in (B): Fourier transform of an ECF_1 crystal formed from ECF_1F_0.

of the other negative stains tested, including uranyl acetate, uranyl oxalate, and methylamine tungstate, yielded two-dimensional arrays with isolated ECF_1 or ECF_1F_0, either alone or in combination with PTA (except when used in the double-staining technique).

ECF_1 arrays were variable in size and degree of crystalline order whether formed from pure ECF_1 or ECF_1F_0. Arrays containing 200 or more molecules were frequent in the best regions of some of the sample grids examined, and most crystals were composed of single domains, or in some cases small numbers of domains separated by clearly visible dislocations. Areas chosen for image analysis consisted on average of about 300 molecules.

Ordered arrays obtained from either ECF_1 or ECF_1F_0 had identical unit-cell dimensions (102 ± 2 Å) and similar appearance, both in the micrographs and in projection maps obtained by image analysis. The crystalline areas seen in ECF_1F_0 preparations thus appear to be composed of only ECF_1, and not F_0. This conclusion is supported by three-dimensional reconstruction of the arrays, which fails to show any sign of F_0.

Image Processing of Micrographs of the ECF_1 Crystals. Optical diffraction patterns of untilted images containing $\gtrsim$100 unit cells routinely showed clear spots to the (1,2) reflections (Figure 1B, inset). Occasional deviations from 6-fold symmetry were invariably attributable to astigmatism or other optical artifacts. Better ordered crystals yielded diffraction patterns occasionally extended to the (1,3) reflections, though with a significant drop in intensity for the higher orders. All images exhibited a single handedness in their diffraction patterns [e.g., (1,2) intensity always greater than (2,1)] when a consistent orientation of specimen and micrograph was maintained. This observation suggests that the orientation of particles on the grid surface (facing up or down) is critical for crystallization and that all arrays are oriented in the same way.

Fourier analysis of the best-ordered images confirmed the 6-fold projection symmetry of the crystals, yielding average phase errors of 18° for all nonzero reflections to the (1,3) (24-Å resolution) and 11° for the stronger, better measured spots to 35-Å resolution, i.e., the (1,2) spots. The interpolative procedure used to compensate for lattice disorder (Henderson et al., 1986) did not alter the resolution of the Fourier transforms, but rather sharpened the reflections and made amplitude and phase estimation for the weak higher order spots more precise and reliable. The amplitudes of symmetry-related spots showed no systematic deviations from *p6* symmetry. Projection maps calculated from unsymmetrized or *p6*-averaged amplitudes and phages (latter data in Table I) invariably showed a strong peripheral 6-fold modulation around a featureless, stain-excluding center (Figure 2). The apparent maximum size of the F_1 in projection is 85–95 Å, depending on the choice of contour level to define the edge of the molecule.

Table I: Amplitudes and Phases of *p6*-Averaged Untilted Projection Images

h,k	amplitude (SD)[a]	phase
1,0	1000 (35)	0
1,1	223 (43)	π
2,0	71 (9)	0
1,2	289 (26)	0
2,1	55 (22)	π
3,0	41 (12)	π
2,2	41 (17)	π
1,3	36 (9)	π
3,1	19 (13)	π

[a] Standard deviations calculated from variability among the six images averaged.

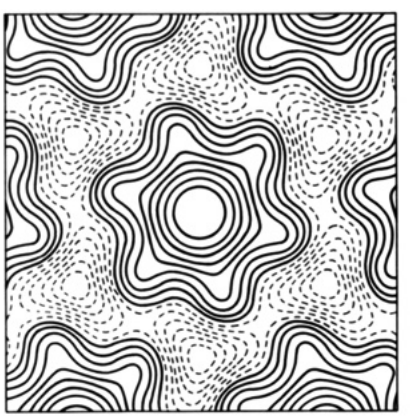

FIGURE 2: Calculated projection map of untilted ECF_1 arrays, displayed as a contour plot (solid lines represent stain-excluding areas). Full width of the figure represents 160 Å.

Combination of data from images of tilted specimens was constrained to *p3* rather than *p6* symmetry, in case the

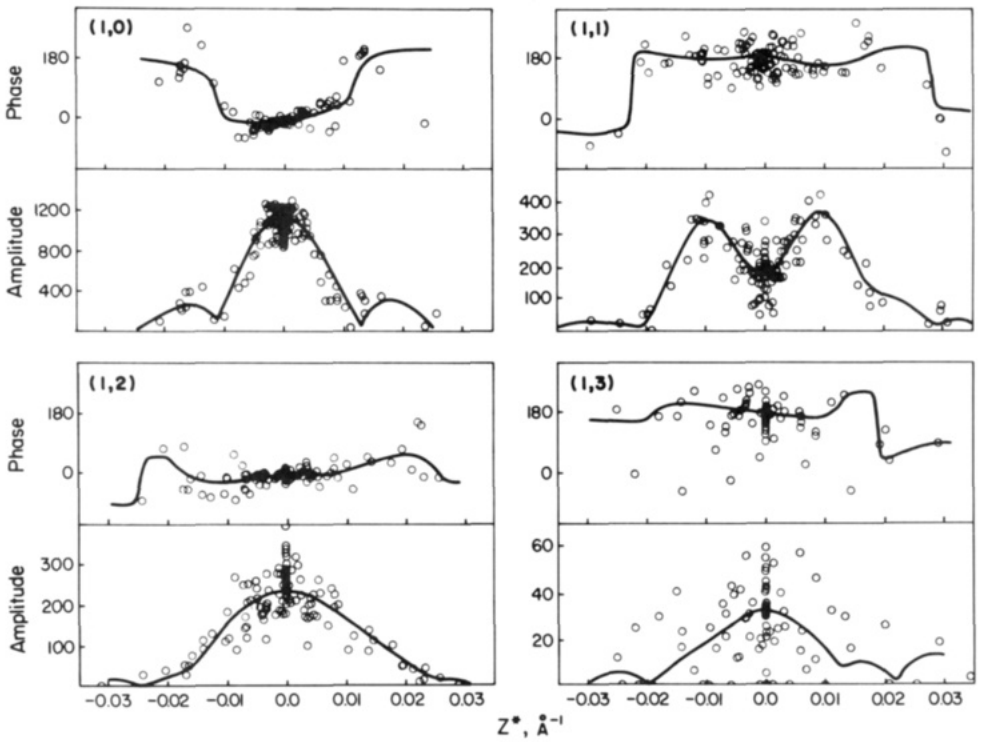

FIGURE 3: Representative data from tilted crystalline ECF_1, displayed with calculated smooth fits to show the variations in amplitude and phase along lattice lines. Note the approximate mirror symmetry of the curves about $z^* = 0$, indicating that the data, combined in the *p3* space group, are close to the higher *p6* symmetry.

three-dimensional structure of the F_1 did not have as high a degree of symmetry as its projection. Forty-four images, including seven from untilted specimens, were included in the amplitude and phase combination. Phase comparisons done over a range of 0.00125 $Å^{-1}$ along lattice lines gave errors ranging from 9° to 32° for the images, in general rising only slightly with tilt angle (e.g., phase errors of 18° for untilted images, 21° for all images). Representative examples of the merged data, together with fitted curves, are shown in Figure 3. As evident from the approximate 2-fold symmetry of the curves about the origin ($z^* = 0$), only minor deviations from *p6* symmetry are apparent.

Three-Dimensional Model of ECF_1 from the Negatively Stained Arrays. A three-dimensional map of the ECF_1 was calculated from the *p3*-merged Fourier terms, allowing a pseudo unit cell of 200 Å in the *z* direction (normal to the crystal plane) to prevent overlap of the structure in the calculation. A region of continuous positive density spanning 90 Å in the *z* direction is located near the center of the map, including 65 Å exhibiting strong 6-fold modulations similar to the projection map. This central region is capped at either end by ~15 Å of weakly 3-fold modulated density. A molecular model of the structure was made, choosing a contour level enclosing a volume of 470 000 $Å^3$ (equal to a molecular mass of 385 000, assuming a protein density of 1.3 g/cm^3) (Figure 4). The most obvious feature of the model is the presence of six elongated lobes, equal in size, which are parallel to the 3-fold axis (tilted from it by less than 5°). These lobes can be traced for most of the length of the F_1. The maximum dimension of this structure in the lateral direction (the plane of the hexagonal sections) is 90 Å.

The contour level chosen as the defining edge of the model in Figure 4 takes into account only the total volume of the subunits. Any internal cavities not penetrated by the stain (see Discussion) are not included in this calculation. Hidden aqueous spaces can be taken into account by increasing the molecular volume. A modest increase in volume, e.g., 20%,

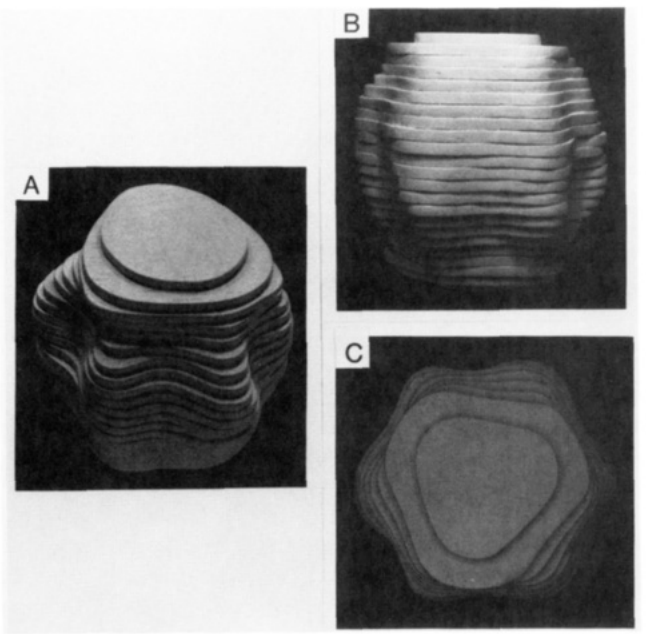

FIGURE 4: Three-dimensional model of ECF_1 derived from analysis of tilted crystalline specimens stained with PTA. Tilted view in (A) shows the longitudinal invaginations of the molecule. Though the top sections [visible in (A) and (C)] show 3-fold variation induced by the *p3* symmetry imposed on the data, the structure is quite clearly 6-fold symmetrical. Both the height of the structure (B) and its maximum width (C), when contoured to give the known molecular weight, are equal to 90 Å (but see Discussion).

does not greatly alter the shape of the negatively stained outline, increasing its lateral dimension to ~95 Å, but not significantly increasing the "height", which remains close to 90 Å.

Cryoelectron Microscopy of ECF_1. As an alternative to negative staining, specimens of ECF_1 were embedded in a thin layer of ice and examined by cryoelectron microscopy. Two-dimensional crystals of ECF_1 were not found in samples

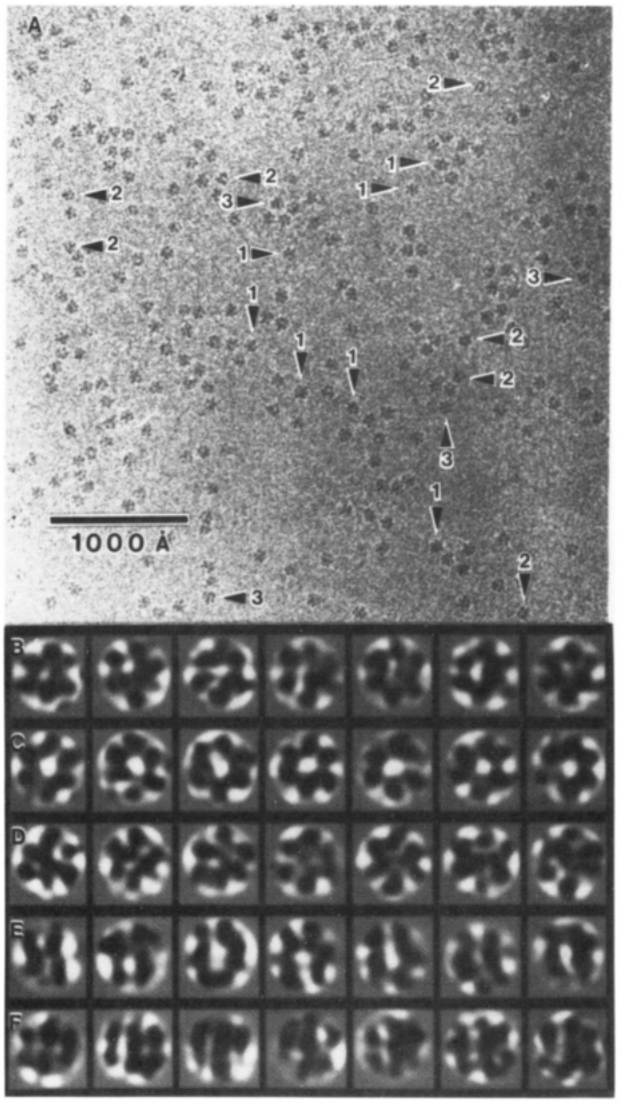

FIGURE 5: (A) Electron micrographs of unstained ECF_1 molecules embedded in a film of amorphous ice. Among the projection views identifiable in this field are (1) hexagonal, (2) bilobed, and (3) trilobed molecules. Galleries of individual images of hexagonal views are shown in (B), (C), and (D) after low-pass filtration to remove high-frequency (<20 Å) noise; the other two categories are illustrated by the particles in (E) and (F).

studied in ice. However, structural information complementary to that derived from the negatively stained two-dimensional crystalline preparations was obtained by analysis of images of the single ECF_1 particles.

A cryoelectron micrograph of a typical field of ECF_1 molecules is shown in Figure 5A, along with a gallery of individual molecules enlarged to show the range of views observed. The micrograph in Figure 5 was underfocused by 0.9 μm (first contrast transfer function zero ~21 Å) as a compromise between resolution limitation and optimal particle contrast. Micrographs used for image processing were all taken at minimum electron doses.

Analysis of Individual ECF_1 Images. The ECF_1 molecules embedded in ice are not constrained to any particular orientation, as is the case with molecules in a two-dimensional array or particles adsorbed to a carbon-coated grid. Therefore, each field contains a variety of projection views of the molecule, all of which were included in the initial particle selection. Preliminary visual inspection identified three distinctive categories of projections: hexagonal (Figure 5B–D), bilobed (Figure 5E), and trilobed (Figure 5F). Approximately 25%

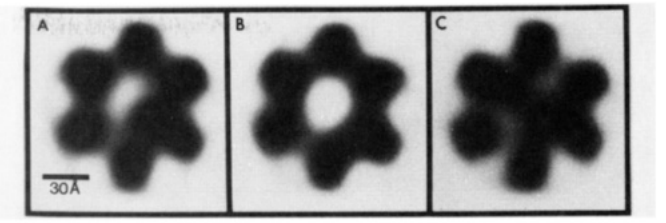

FIGURE 6: Averaged projection images of unstained ECF_1 with hexagonal outlines, displayed with higher density (protein) as dark. Averages are of (A) 63 images displaying an asymmetric center, (B) 33 images with an open center, and (C) 11 images with a partially occluded center.

of the images could be readily sorted into these three categories; the remainder either were not clear enough to allow classification, did not have distinguishable features, or were present in very low frequency.

Classification of the images was attempted by automated methods, by correspondence analysis. This approach has been successful in the classification of negatively stained protein assemblies (Frank, 1984; Verschoor et al., 1985; Boekema et al., 1986, 1988), which present a more limited number of projections, and with higher contrast, than the unstained images in this work. Use of this method with the ECF_1 data resulted in similar categories of particles (hexagonal, bilobed, and trilobed), along with many other minor classes. The composition of each class was less visually homogeneous than obtained by manual sorting, including diffuse, poorly contrasted particles in each category, along with some evidently dissonant images. This data set of images appears to include a continuum of projections through the ECF_1, perhaps with some views favored (e.g., the hexagonal views), and thus it may be futile to attempt to classify all, or even a majority of the images, into a workable number of categories. Therefore, particularly since the major visually selected categories were reproduced by the more objective analysis, manual sorting into the most frequently seen and readily distinguishable classes of images appears to be the most conservative interpretation of these data.

Individual images in each category were aligned to reference images, as described under Materials and Methods, and averaged. Classification and successful alignment were easiest to assess in the clearest images, those with the highest signal-to-noise ratio. By averaging as few as ~20 of these images, the major features were clearly evident; the phases of Fourier transforms of independent averages of 20 particles were within 45° of each other in incremental rings to a resolution of ~30 Å (Frank et al., 1981b). Addition of images with lower contrast only marginally improved the clarity of the features of the image (as well as the resolution, to ~25 Å), and, therefore, only the clearest, best-aligned images were used (see legends to Figures 6 and 7).

Of the 1400 molecules in the data set, 241 were classified as hexagonal; i.e., they showed a hexagonal arrangement of the peripheral densities around a central aqueous cavity. Most of these (~65%) have an addition density located within the ring of outer densities and distinctly off-center. A gallery of these is shown in Figure 5B, and an average projection of this class is shown in Figure 6A. A smaller fraction of the hexagonal views (~25%) have a more open central cavity, with only a minimal amount of interior density, as shown in the gallery in Figure 5C and the average image in Figure 6B. Another distinctive though rare subcategory (~10% of the hexagonal views) was identified in which the interior of the molecule is occluded by a delocalized central density. Individual images are shown in Figure 5D and an average in Figure

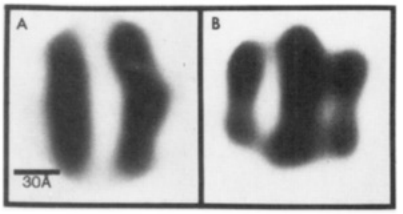

FIGURE 7: Averaged aligned images of 70 bilobed projections (A) and 32 trilobed views (B) of unstained ECF_1.

6C. The maximum diameter of the ECF_1 in the hexagonal projection is 95–100 Å with each of the six peripheral densities 30–35 Å in diameter. The central cavity is 30–40 Å in diameter.

The bilobed and trilobed views of ECF_1, as represented by the galleries of single molecules in Figure 5E,F, were found much less frequently than hexagonal projections. An average image of the bilobed view (Figure 7A) has maximal dimensions of ~90 Å along and ~80 Å across the lobes, each of which is 25–30 Å wide. It is traversed along its entire length by an elongated cavity, ~30 Å wide, which is partially constricted at one end (top in Figure 7A). This constriction, formed by an asymmetric extension of one of the lobes, defines a hand as well as a "top" and "bottom" in this projection of the ECF_1. After alignment, approximately half of the bilobed images were initially mirror images of Figure 7A; i.e., the molecules were turned 180° in the plane of the ice film compared to the remainder. These images were mirrored about an axis along the lobes in order to be included in the average.

Trilobed views of ECF_1 were identified with only about half the frequency of the bilobed views. Like the bilobed view, the dimension along the lobes of the average in Figure 7B is ~90 Å, but it appears slightly wider (~90 Å). The cavities between the lobes are not as wide or pronounced as in the bilobed view.

The single-particle views of the unstained ECF_1 can be understood as projections of a model of the three-dimensional structure. The schematic representation in Figure 8 incorporates a cavity at the center of the molecular outline determined from analysis of the negatively stained crystals. Six elongated subunits around the periphery define a channel-like cavity through the length of the structure. The cavity is partially occluded at one end by a compact protein density, which is partially located within the ring of the outer subunits, asymmetrically close to one of them.

The different hexagonal projections can be explained as views from the ends of the structure, over a range of tilt angles small enough not to distort significantly the hexagonal shape. The bilobed and trilobed views are interpretable as projections from the side of the structure, along lines of sight either between the clefts separating subunits or centered on the subunits (arrows in Figure 8). Both of these side views allow substantial tilts along the long axis of the subunits without obscuring the essential features of the projections and have a triple degeneracy in lines of sight through the structure, thus ensuring a significant sampling of these projections in the data set. Other projections are likely to be present in the data set but either fail to superimpose protein density in a distinctive way or else have a very small range of viewing angles, severely restricting their representation among all possible images.

Discussion

This structural study of the ECF_1 has combined three-dimensional analysis of negatively stained two-dimensional crystals with single-particle analysis of the unstained enzyme embedded in a thin layer of amorphous ice. The crystal data provide a molecular outline of the protein but do not reveal

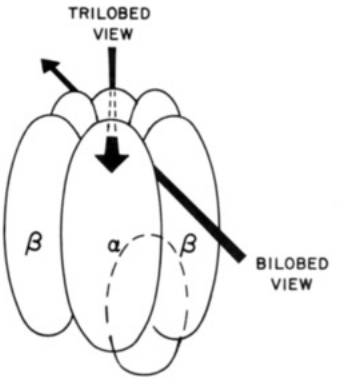

FIGURE 8: Schematic model of ECF_1 derived from projection views of the unstained molecule (Figures 6 and 7), interpreted in the framework of the three-dimensional stain-excluding outline (Figure 4). The directions of view which produce the bilobed and trilobed projections are indicated. The peripheral subunits are presumed to be the α and β subunits, and the smaller density interior to them probably consists of at least parts of the γ, δ, and/or ϵ subunits.

features of the interior of the structure. The images obtained in ice clearly show an aqueous cavity at the center of the molecule and provide information about subunit shapes and locations.

Two-dimensional crystals of ECF_1 were obtained by using either purified soluble ECF_1 or membrane-bound ECF_1F_0 as the starting material. These crystals are formed when the protein is negatively stained with PTA but not when other stains are used. Negative staining embeds the specimen in a layer of amorphous heavy-metal salt, providing a high level of electron contrast between the protein and the surrounding aqueous phase, along with physical support and some degree of protection from radiation damage.

A three-dimensional model of ECF_1 was constructed from data collected from tilted specimens. Only two exposures were taken with any specimen, one at a zero or low tilt angle, and these were done under low dose conditions to minimize radiation damage. Our model of the enzyme is a roughly spherical structure. The diameter of the protein in the hexagonal (top) view of Figure 4 is 90–95 Å, and the height (side view) is 90 Å. The model was constructed by choosing a contour level to include a molecular volume equal to a mass of 385 000, because PTA did not penetrate the interior of the molecule to reveal any aqueous volume. Electron micrographs of the enzyme in ice clearly show a central cavity; enlarging the model to accommodate the extra volume of this cavity increases the diameter to ~95 Å, without significantly changing the height.

The diameter of the molecule obtained from negatively stained crystals is close to that measured from the hexagonal projection in ice, 95–100 Å. The height of 90 Å is very similar to that obtained for the molecule in side views of the isolated ECF_1.

It is not clear whether the ECF_1 crystallized after stripping from F_0 contains a full complement of subunits. The same is true of the ordered arrays obtained with purified ECF_1, which, for example, may have lost the labile δ and ϵ subunits during the staining procedure. This issue was not addressed because the structure obtained from the two-dimensional crystals describes only the large (α and β) subunits, and not the smaller components.

The axial ratio of our structure is close to 1, substantially smaller than indicated by previous electron microscopy studies. Tsuprun et al. (1984) reported the diameter of the hexagonal projection as 105 Å, close to our values, but the height as only 60 Å. The latter dimension was measured from views of the

F_1 molecule containing only four protein densities, which were interpreted as side views of the structure. Our data set of ECF_1 molecules in ice includes similar images but in insufficient numbers to warrant interpretation. Tiedge et al. (1983) reported the diameter of the hexagonal projection in their micrographs as 108–123 Å and a height calculated from a tilt series of individual molecules of F_1 as only 60 Å. No correction was made for the change in stain thickness with the angle of tilt. Moreover, the tilted images were recorded with multiple exposures at high electron doses which can cause substantial specimen flattening (Berriman & Leonard, 1986; Jesoir & Wade, 1987).

The major feature resolved in the structure determination from the negatively stained two-dimensional crystals is a hexagonal modulation of the molecule. A hexagonal arrangement of densities identified as the α and β subunits has been seen in projection images of single molecules in stain (Akey et al., 1983; Tiedge et al., 1983; Tsuprun et al., 1984; Boekema et al., 1986, 1988). In three dimensions, these peripheral subunits are elongated structures, interdigitated for most of the height of the ECF_1 molecule. Only near the ends of the molecule does the 6-fold modulation disappear. Antibody binding experiments show that the α and β subunits alternate at the periphery of the F_1 molecule (Lünsdorf et al., 1984; Tiedge et al., 1985; Gogol et al., 1989). The cleft between neighboring α and β subunits is most prominent near the center of the structure.

Our picture of ECF_1 is very different from models proposed by Tsuprun et al. (1984) and Tiedge et al. (1983), in which the α and β subunits are roughly spherical and arranged in two layers, with little or no interdigitation. The limitations of these studies have been noted above. It is also at variance with the model proposed by Amzel et al. (1982), based on a preliminary interpretation of X-ray crystal data at a resolution of 9 Å, which has two distinct layers of subunits. A two-layered arrangement of subunits is difficult to reconcile with our data, unless the two-dimensional crystals of ECF_1 are random mixtures of molecules in different orientations, differing by 60° rotations. If this mixture were present, equivalent intermolecular contacts would be made by α–α, α–β, and β–β subunit pairs on neighboring molecules. This possibility is even more unlikely for a two-tiered structure, which would require identical random contacts, regardless of the position (top or bottom layer) of the subunits.

Use of frozen hydrated specimens is a recent innovation in the study of protein structure, applicable both to ordered arrangements of protein as well as to single particles of large complexes. Our study is the first to apply this technique with single-particle analysis to a protein as small as ECF_1. The major advantages of this method are the preservation of native structures by rapidly freezing in suitable buffers and direct visualization of the protein density rather than its outline defined by stain exclusion. Contrast between specimen (protein) and background (water) is much less than with stained samples, so the signal-to-noise ratio is lower, and image averaging is needed to define molecular details.

The hexagonal view of ECF_1 in ice shows the α and β subunits end-on with respect to the model in Figure 4, clearly differentiated both from the surrounding aqueous phase and from the aqueous interior of the structure. The diameter of the large subunits in this projection is ~35 Å, which suggests a length of close to 90 Å on the basis of their molecular weights (~55 000). This length can be accommodated only if the α and β subunits are interdigitated through most of the height of the molecule.

It has been reported that F_1 contains a space within the structure that is penetrated by the negative stain uranyl acetate (Boekema et al., 1986, 1988) although not by PTA (this study). Projections of ECF_1 in ice confirm the presence of an internal aqueous cavity. Side views of the molecule suggest that the cavity extends through the entire structure.

The bilobed view is interpreted as a side view of ECF_1, based on a comparison with the three-dimensional model (Figure 4). More direct evidence that this projection and the trilobed view are side views comes from studies of undissociated ECF_1F_0 in membranes (Lücken et al., unpublished results). Both of these views are frequently found in side views of the ECF_1 part of the ECF_1F_0 complex, visualized at the edges of vesicles or in narrow membrane sheets of the enzyme.

A protein density inside the ECF_1 which partly occludes the central aqueous cavity was visualized in hexagonal projections. It is located off-center in the structure, probably localized to one end, and is most likely composed of one or more of the small subunits of the complex. In most of the hexagonal projections, the internal density is asymmetrically located adjacent to one of the peripheral subunits, similar to the observations of Boekema et al. (1986). In a minority of the hexagonal projections of ECF_1, the central structure appears to be missing, with only a small amount of density added to one of the peripheral subunits. Another small subset of hexagonal views has the entire interior obscured by a less compact density. Similar variability in projections has been reported by Akey et al. (1983) in their study of single molecules of ECF_1 and chloroplast F_1 in negative stain. These workers interpreted the different hexagonal projections to be compositionally different forms of the enzyme, i.e., molecules missing δ and ϵ subunits. This explanation is unlikely to hold for our data, since hexagonal projections of trypsin-cleaved ECF_1, which is missing the δ and ϵ subunits, have a reduced, but clearly evident, internal density, indicating that the γ subunit is a major part of this structural feature (Gogol et al., 1989). The observed variability in hexagonal projections may be due to the presence of several structurally different conformers of the enzyme; more likely, it represents small tilts of the ECF_1 about its hexagonal axis, sufficient to displace the central mass without distorting the outer hexagon.

In our model shown in Figure 8, the internal mass is placed at one end of the structure. This location is consistent with biochemical data which demonstate that the small subunits are sensitive to proteases and can bind antibodies (Dunn et al., 1980; Bragg & Hou, 1987; Gavilanes-Ruiz et al., 1988; Aggeler et al., 1987). The bilobed view of ECF_1 shows a constriction of the aqueous channel at one end which may be the central mass in side projection.

ACKNOWLEDGMENTS

We thank Trisha Ryan and Barbara Robbins for preparation of the ECF_1 and ECF_1F_0 used in this work and Dr. Brian Matthews for use of computer facilities for image analysis.

Registry No. ATPase, 9000-83-3.

REFERENCES

Agard, D. (1983) *J. Mol. Biol. 167*, 849–852.

Aggeler, R., Zhang, Y.-Z., & Capaldi, R. A. (1987) *Biochemistry 26*, 7107–7113.

Akey, C. W., Crepeau, R. H., Dunn, S. D., McCarty, R. E., & Edelstein, S. J. (1983) *EMBO J. 2*, 1409–1415.

Amos, L. A., Henderson, R., & Unwin, P. N. T. (1982) *Prog. Biophys. Mol. Biol. 39*, 183–231.

Amzel, L. M., & Pedersen, P. L. (1983) *Annu. Rev. Biochem. 52*, 801–824.

Amzel, L. M., McKinney, M., Narayanan, P., & Pedersen, P. L. (1982) *Proc. Natl. Acad. Sci. U.S.A. 79*, 5852–5856.
Berriman, J., & Leonard, K. (1986) *Ultramicroscopy 19*, 349–366.
Boekema, E. J., Berden, J. A., & van Heel, M. G. (1986) *Biochim. Biophys. Acta 851*, 353–360.
Boekema, E. J., van Heel, M., & Gräber, P. (1988) *Biochim. Biophys. Acta 933*, 365–371.
Bradford, M. (1976) *Anal. Biochem. 72*, 248–254.
Bragg, P. D., & Hou, C. (1987) *Biochim. Biophys. Acta 894*, 127–137.
Bretaudiere, J. P., & Frank, J. (1986) *J. Microsc. 144*, 1–14.
Brink, J., Boekema, E. J., & van Bruggen, E. F. J. (1988) *Electron Microsc. Rev. 1*, 175–199.
Dunn, S. D., Heppel, L. A., & Fullmer, C. S. (1980) *J. Biol. Chem. 255*, 6891–6896.
Foster, D. L., & Fillingame, R. H. (1979) *J. Biol. Chem. 254*, 8230–8236.
Foster, D. L., & Fillingame, R. H. (1982) *J. Biol. Chem. 257*, 2009–2015.
Frank, J. (1984) *Ultramicroscopy 13*, 153–164.
Frank, J., Shimkin, B., & Dowse, H. (1981a) *Ultramicroscopy 6*, 343–358.
Frank, J., Verschoor, A., & Boublik, M. (1981b) *Science 214*, 1353–1355.
Gavilanes-Ruiz, M., Tommasino, M., & Capaldi, R. A. (1988) *Biochemistry 27*, 603–609.
Gogol, E. P., Lücken, U., & Capaldi, R. A. (1987) *FEBS Lett. 219*, 274–278.
Gogol, E. P., Aggeler, R., Sagermann, M., & Capaldi, R. A. (1989) *Biochemistry* (following paper in this issue).
Henderson, R., Baldwin, J. M., Downing, K. H., Lepault, J., & Zemlin, F. (1986) *Ultramicroscopy 19*, 147–178.
Jesoir, J.-C., & Wade, R. H. (1987) *Ultramicroscopy 21*, 313–320.
Kagawa, Y., Nobuhito, S., Yoshida, M., Hirata, H., & Okamoto, H. (1976) *J. Biochem. 80*, 141–151.
Lötscher, H. R., de Jong, C., & Capaldi, R. A. (1984) *Biochemistry 23*, 4128–4134.
Ludwig, B., Prochaska, L., & Capaldi, R. A. (1980) *Biochemistry 19*, 1516–1523.
Lünsdorf, H., Ehrig, K., Friedl, P., & Schairer, H. U. (1984) *J. Mol. Biol. 173*, 131–136.
Racker, E., Horstman, L. L., Kling, D., & Fessenden-Raden, J. M. (1969) *J. Biol. Chem. 244*, 6668–6674.
Schneider, E., & Altendorf, K. H. (1985) *EMBO J. 4*, 515–518.
Senior, A. E. (1988) *Physiol. Rev. 68*, 177–231.
Stewart, M., & Vigers, G. (1986) *Nature 319*, 631–636.
Tiedge, H., Schäfer, G., & Mayer, F. (1983) *Eur. J. Biochem. 132*, 37–45.
Tiedge, H., Lünsdorf, H., Schäfer, G., & Schairer, H. U. (1985) *Proc. Natl. Acad. Sci. U.S.A. 82*, 7874–7878.
Tsuprun, V. L., Mesyanzhinova, I. V., Kozlov, I. A., & Orlova, E. V. (1984) *FEBS Lett. 167*, 285–290.
van Heel, M., & Keegstra, W. (1981) *Ultramicroscopy 7*, 113–130.
Verschoor, A., Frank, J., & Boublik, M. (1985) *J. Ultrastruct. Res. 92*, 180–189.
Vignais, P. V., & Satre, M. (1984) *Mol. Cell Biochem. 73*, 105–124.
Vignais, P. V., & Lunardi, J. (1985) *Annu. Rev. Biochem. 54*, 977–1014.
Wagenknecht, T., Grassucci, R., & Frank, J. (1988) *J. Mol. Biol. 199*, 137–147.
Walker, J. E., Saraste, M., & Gay, N. J. (1984) *Biochim. Biophys. Acta 768*, 164–200.
Wise, J. G., Latchney, L. R., Ferguson, A. M., & Senior, A. E. (1984) *Biochemistry 23*, 1426–1432.